Magnetostrictive Domain Walls in Antiferromagnetic NiO

N. B. Weber and H. Ohldag*
Institut für Angewandte Physik, Heinrich-Heine-Universität Düsseldorf, 40225 Düsseldorf, Germany
H. Gomonaj† and F. U. Hillebrecht‡
Max-Planck-Institut für Mikrostrukturphysik, Weinberg 2, 06120, Halle, Germany
(Received 16 October 2002; published 5 December 2003)

We report high-resolution observations of antiferromagnetic (AF) domain walls at the surface of NiO and determine the typical width of AF walls in this material to be of the order of 150 nm. We observe a number of different types of domain walls, including double walls caused by long-range interaction between walls. We describe the observed wall profiles by a model containing the exchange interaction and magnetostriction as basic ingredients. The good agreement of this model with experiment shows that the formation of walls between antiferromagnetic domains in NiO and their properties are dominated by magnetoelastic interactions.

DOI: 10.1103/PhysRevLett.91.237205 PACS numbers: 75.50.Ee, 75.60.Ch

Domain walls (DW) in antiferromagnets are often described on the same basis as the domain walls in ferromagnets. The analogy arises from the fact that on a macroscopic scale both structures can be characterized by a single vector (the magnetization for ferromagnets, and the antiferromagnetic (AF) vector, i.e., the *difference* between the two sublattice magnetizations, for antiferromagnets) whose origin is governed by strong exchange interactions, and whose orientation is defined by a local anisotropy field. This description is appropriate and sufficient for walls separating domains with different orientations of the magnetic vectors. However, while for ferromagnets this is the only possible type of domain wall, a much wider variety of configurations is possible for AF crystals in which magnetic ordering is related not only to an appearance of a new vector but in addition to a change of the crystal translational symmetry. Since the properties of domain walls provide a key to understanding the magnetic microstructure [1], experimental determinations of their properties are extremely important. Until recently, such high-resolution observations were possible only for ferromagnetic domain walls, e.g., by Lorentz microscopy [2] or photoemission microscopy using magnetic circular dichroism [3]. The first observations of certain antiferromagnetic walls were achieved by spin-polarized scanning tunneling microscopy on Cr single crystal surfaces [4,5]. In this Letter, we present the first high-resolution study of antiferromagnetic domain walls in NiO by photoemission microscopy combined with linear magnetic dichroism.

The images were obtained in the PEEM 2 photoemission microscope installed at beamline 7.3.1.1 of the Advanced Light Source, Berkeley National Laboratory [6]. In photoemission microscopy, the absorption coefficient is measured in a spatially resolved way via the total yield of electrons released from the sample as a result of irradiation by UV or soft x-ray photons. For NiO, the Ni $2p_{1/2}$ absorption edge occurring at 874 eV photon energy shows a double peak arising from the influence of large Coulomb and exchange interactions [7]. The relative strength of the two peaks depends on the angle θ between (linear) light polarization and the direction of magnetic moments of the form $(3\cos^2\theta - 1)$ [8]. This linear dichroism is used for imaging antiferromagnetic structures [9–11]. From measurements on e-beam lithography test samples, we estimate the resolution to about 50 nm. The sample was a bulk crystal, from which a fresh (100) surface was exposed by *ex situ* cleavage immediately before introduction into the microscope.

Because of the $\cos^2\theta$ dependence, the two sublattices within a single domain yield the same absorption spectrum [8]; however, different domains are distinguishable [9–11]. A typical domain pattern observed on a NiO(100) surface is shown in Fig. 1(a). The domains appear as stripes parallel to the [100] and [110] directions within the surface [10]. In a previous study of AF domains on NiO(100) by photoemission microscopy, we found from the dependence of the AF domain contrast on azimuthal sample orientation that the spin structure at the surface is essentially bulk terminated [11].

The contrast between domains disappears whenever the angle θ is the same for two neighboring domains [11]. This is the case for light polarization parallel or perpendicular to the domain walls, as shown in Fig. 1(b). Although the contrast between the domains themselves has disappeared, the image shows narrow lines, which by comparison to the domain image can be identified as domain walls. The domain walls running parallel to the $\langle 100 \rangle$ directions appear *brighter* than the domain areas, whereas the $\langle 110 \rangle$ walls appear *darker* for the sample orientation shown. The wall contrast demonstrates that in the AF domain wall the AF vector rotates *within* the surface plane, rather than rotating out of the surface. Therefore, one can characterize the (100) walls between T domains as Néel type, where the antiferromagnetic vector rotates *through* the plane of the wall.

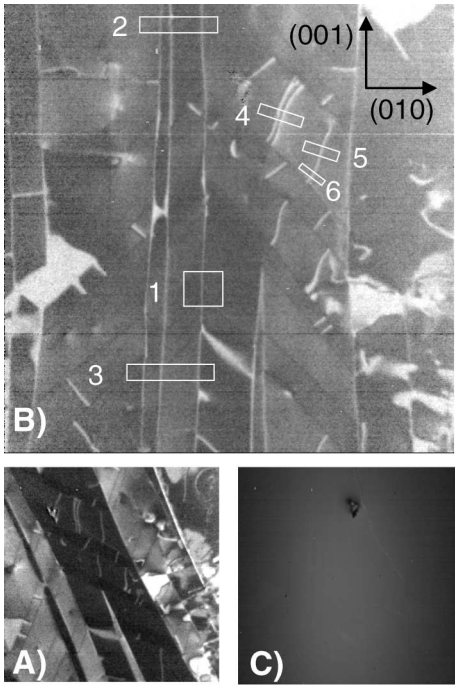

FIG. 1. Antiferromagnetic domain walls on the NiO(100) surface imaged by photoemission microscopy. The contrast between domains (a) disappears when the light polarization is parallel to a [010] direction within the surface (b). In this situation, there is only contrast due to the domain walls. The walls running along [001] appear brighter; walls parallel to $[0\bar{1}1]$ or [011] appear darker than the inner of the domains. (c) An topography image formed from the mean PEEM intensity obtained at 871 and 872 eV shows no features which may influence the domain structure, and shows that all the features seen in (a) and (b) are of magnetic origin. The field of view is about $35 \times 35\ \mu\text{m}^2$.

In Fig. 1(b) some regions have been marked, from which wall profiles in Fig. 2 have been derived. The top panel shows two profiles of a wall running approximately along ⟨100⟩, taken at different locations along the wall. The width (FWHM) of this particular wall varies between 134 and 184 nm [12]. The uncertainty arising from finite resolution, pixel size, and averaging along the wall is about ±20 nm. The variation of the wall width both for a single wall as well as from one wall to another is presumably caused by the influence of local stresses due to crystal defects.

Figure 1(b) also shows another type of DW, separating regions which appear with the same contrast under all light polarizations or sample orientations (regions 4–6). Therefore, the domains on both sides are identical. However, to be visible the spin orientation in the walls has to deviate from that in the adjacent domains. A possible interpretation for these walls is as faults of the AF stacking of the (111) planes (or an antiphase boundary). The spins then reorient themselves within the set of (111) planes of the T domain via a rotation of the spins within these planes. The width of these walls is slightly larger than those of the T walls discussed above. The

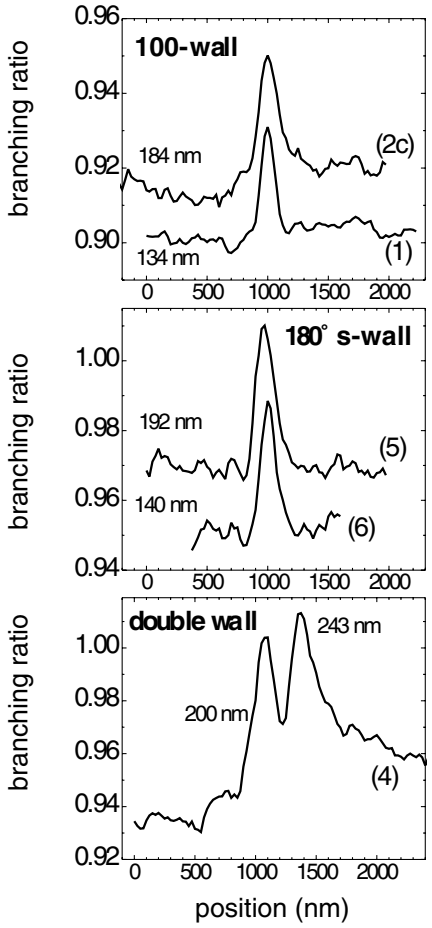

FIG. 2. Profiles through some of the domain walls observed on NiO(100); the numbers in brackets refer to the regions marked in Fig. 1(b). Widths (FWHM's) are given in nm near the profiles. (a) Wall running roughly parallel to 001; (2c) refers to the right wall in region 2, i.e., the same one as 1 at a different location. (b) Curved walls running between two $(0\bar{1}1)$ walls; the profile for (5) was offset by adding 0.02 to the branching ratio. (c) Profile for double wall. Widths derived from other profiles are given in Ref. [12].

directions of these walls are not tied to low index crystallographic directions. Figure 2 shows profiles for one of these walls, which yield a width between 140 and 192 nm. The lower panel of Fig. 2 shows a profile of the double wall seen in Fig. 1(b).

The structure and orientation of AF domain walls are governed mainly by the rather large magnetostrictive strains ranging from 10^{-3} for the rhombohedral deformation [13] to nearly 10^{-4} for the deviatory distortion in the (111) planes [14]. A plane infinite T wall with normal $\mathbf{n}$ separating two domains with different AF vectors and corresponding spontaneous strain tensors $\hat{\mathbf{u}}^{(1)}$ and $\hat{\mathbf{u}}^{(2)}$ is a source of elastic long-range distortions [15] which relax the incompatibility $\hat{\boldsymbol{\eta}}$ of the deformations:

$$\hat{\boldsymbol{\eta}} \equiv -\mathbf{n} \times (\mathbf{u}^{(1)} - \mathbf{u}^{(2)}) \times \mathbf{n}. \quad (1)$$

If the incompatibility $\hat{\boldsymbol{\eta}}$ has a magnitude comparable to the magnetostriction itself, its contribution to the free

energy density, $f_{\mathrm{inc}} \propto \hat{\eta}\hat{c}\,\hat{\eta}$ ($\hat{c}$ is the tensor of elastic moduli), competes with the energy of the bare magnetic anisotropy. This imposes certain restrictions on the DW's and governs their shape and orientation.

For walls separating T domains, the optimal orientation of the DW plane for which the incompatibility (1) vanishes is (110) or (100). This is evident in Fig. 1(b), where T walls appear only with these orientations. Any other orientation will produce elastic strains whose contribution to the crystal energy density can rise to 10^5 J/m^3, which is comparable to the out-of-plane anisotropy 3.32×10^5 J/m^3 [16]. We conclude that the observed AF domain pattern is of elastic origin.

The deformations associated with the AF state have to match at domain walls, which influences the shape of AF domain walls. The simultaneous variation of the AF vector and the associated magnetically induced deformation inside the walls is a source of incompatibilities (that can be thought of as quasidislocations [15]) and thus is energetically disadvantageous. The energy increase can be avoided if the strains inside the DW are frozen, i.e., take a constant value ($\mathbf{u}^{(1)}$ or $\mathbf{u}^{(2)}$) inside the domain, and change in a stepwise manner at the center of the DW. Therefore, the strains contribute to the anisotropy, which favors orientation of magnetic moments within the given (111) plane. This can be accounted for by replacing the bare magnetic anisotropy by an effective one of the form

$$\beta_{\mathrm{eff}}^{(2)} = \beta_{\parallel}^{(2)} - \frac{\Lambda\lambda_{44}}{2c_{44}}. \tag{2}$$

The crystal-field magnetic anisotropy $\beta_{\parallel}^{(2)}$ and the additional magnetoelastic contribution induced by the frozen strains, $\Lambda\lambda_{44}/2c_{44}$, are of comparable magnitude. In (2), the magnetoelastic constant Λ arises from the dependence of the exchange integral on interatomic separation, and λ_{44} is the relevant magnetoelastic constant, which relates the shear strain with the orientation of the AF vector.

The structure of the DW is governed mainly by the competition between the exchange interaction, which favors collinear alignment of the antiferromagnetic moments, and the *effective anisotropy* defined by Eq. (2). This is the essence of what distinguishes the antiferromagnetic walls discussed here from the commonly encountered domain walls in ferromagnetic materials where the magnetic anisotropy is uniform throughout the sample and across the wall.

Within the model laid out above we have calculated the profile of the wall separating the domains with a different direction of AF exchange coupling. In contrast to the previous model developed by Yamada [17](which addresses a different geometry) we assume that spins in different sublattices are kept in parallel almost throughout the DW, thereby significantly reducing the exchange energy. For the position dependence of the AF vector $\mathbf{L}$ for a Néel-type (100) wall (illustrated schematically in Fig. 3, inset) we obtain

$$L_x = \frac{1 + \sqrt{6}|\sinh(\xi/\xi_0)| + 2\cosh(\xi/\xi_0)}{3\cosh(\xi/\xi_0) + \sqrt{6}|\sinh(\xi/\xi_0)|},$$
$$L_y = L_z = \frac{\mathrm{sgn}\,\xi}{\sqrt{2}} \frac{\sqrt{3}|\sinh(\xi/\xi_0)| + \sqrt{2}[\cosh(\xi/\xi_0) - 1]}{3\cosh(\xi/\xi_0) + \sqrt{6}|\sinh(\xi/\xi_0)|}, \tag{3}$$

where ξ is a coordinate perpendicular to the DW plane. α is the exchange stiffness constant, and $\xi_0 = [\alpha/\beta_{\mathrm{eff}}^{(2)}]^{1/2}$ can be considered as the DW half-width. The calculated wall profile as represented by the projection of the antiferromagnetic vector on the direction normal to the plane of the wall is shown in Fig. 3 as a solid line. From the modeling we extract the magnitude of ξ_0 to be 73 nm; using $\alpha \cong 3 \times 10^{-11}$ J/m yields $\beta_{\mathrm{eff}}^{(2)} = 0.57 \times 10^4$ J/m^3 for the effective magnetic anisotropy. This contribution is comparable to the magnetoelastic coupling of $\Lambda\lambda_{44}/2c_{44} \propto 10^4$ J/m^3 (calculated from the trigonal distortion $\Delta = 1.3 \times 10^{-3}$ [13], shear strain -9.5×10^{-5} in the $[11\bar{2}]$ direction [18], and shear modulus $c_{44} 1.1 \times 10^{12}$ [19]). This demonstrates not only the role of magnetoelastic coupling in the formation of the DW structure, which was first noted by Yamada, but also reveals the nature of the related forces. The exchange interaction represented by the constant Λ is insensitive to the orientation of the AF vector with respect to crystal axes and cannot itself be responsible for the rotation of $\mathbf{L}$ inside the domain wall. Without taking into account the anisotropic magnetoelastic coefficient λ_{44} which arises from direction-dependent spin-orbit coupling, an *unrealistically small* width of the wall, 8 nm, would be obtained, with an energy of 4×10^{-3} J/m^2 [17]. In our model we obtain a domain wall energy of 4.2×10^{-4} J/m^2 [20].

The observed Bloch-type DW separating different S domains is described by an expression similar to (3).

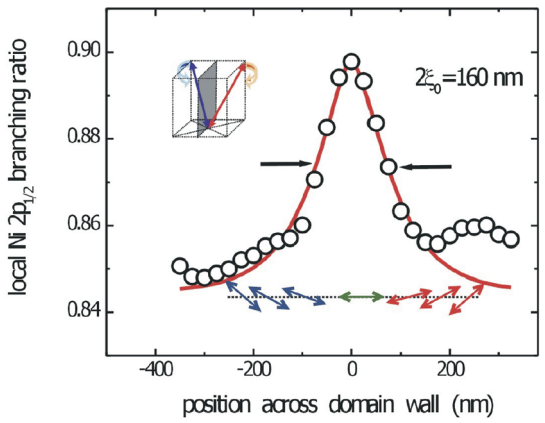

FIG. 3 (color online). Profile of a T domain wall in Fig. 1(b), averaged along the wall in region 1. Points, experimental data; solid line, calculated from (3) with $\xi_0 = 73$ nm. The width (FWHM) of the AF domain wall is about 160 nm. The inset shows a schematic representation of the (001) domain wall. Double-ended arrows show orientation of the AF vector inside the DW.

However, the wall width is defined by the weaker in-plane anisotropy of magnetoelastic origin, $(\lambda_{11} - \lambda_{12})^2/12(c_{11} - c_{12})$. Correspondingly, the wall should be wider, nearly 200 nm, in agreement with the experimental data. Considering only the bare magnetic anisotropy, a much *larger* width would be obtained because of the small in-plane anisotropy.

So far we have considered only the idealized situation of isolated walls between infinitely large domains. However, the complex domain structure shows evidence that domain walls interact with each other. Examples are spots where [110] walls end at a [100] wall, leading to a kink in the latter one, or also the interconnect between the two left walls of regions 1 and 3 in the middle of the image. The most striking cases are the curved walls of regions 4–6. The internal stresses induced by the large magnetostriction of NiO arise at points where different DW's form a junction. The magnetostrictive distortion produces not only strain but also a *rotation* of the crystal lattice with respect to the nondeformed paramagnetic state. Accumulation of the rotations in the vicinity of the DW junction generates a disclination, which can be thought of as a wedge-shaped lack or excess of material. The continuity of the sample is then achieved by long-range stresses and corresponding strains. In antiferromagnetic NiO, disclinations should always occur at junctions of S and T walls and strongly influence their shape and position. Two disclinations positioned at the same T-T boundary have opposite signs (the positive sign of disclination corresponds to a lack of the material) and thus attract each other. Such an attractive interaction is observed between the pair of the S-S domain walls seen in the upper right corner in Fig. 1(b). The disclinations locked at opposite sides of a T domain have opposite signs and try to get as close as possible. The S-S domain wall, which connects these disclinations, tends to align itself parallel to the easy direction and thus forces the disclinations apart. The competition between these two factors results in a bending of the domain wall, as seen in experiment.

In summary, we have reported the first direct observation of antiferromagnetic domain walls on the NiO (100) surface. From the experimental data, T walls are found to be about 150 nm wide, in contrast to early estimates producing much smaller widths. Modeling shows that *magnetoelastic interaction* is the primary factor governing the width, internal structure, and interaction between walls. Our model is applicable to any antiferromagnet with strong magnetoelastic coupling. In particular, it can be applied to CoO with only a slight modification, but also to underdoped superconductors which have an antiferromagnetic ground state.

The help of A. Scholl, Advanced Light Source, in the operation of the photoemission microscopy facility is gratefully acknowledged. H. G. and F. U. H. are grateful to J. Kirschner and D. Sander of MPI Halle for critical discussions.

*Present addresses: Stanford Synchrotron Radiation Laboratory, P.O. Box 20450, Stanford, CA 94309, USA; Advanced Light Source, Lawrence Berkeley National Laboratory, One Cyclotron Road, Berkeley, CA 94720, USA.

†Permanent address: National Technical University "KPI," ave Peremogy, 37, 03056 Kyiv, Ukraine.
Email address: malyshen@ukrpack.net

‡Present address: Institut für Festköperphysik, Forschungszentrum Karlsruhe, P.O. Box 3640, 76021 Karlsruhe, Germany.
Email address: Ulrich.Hillebrecht@ifp.fzk.de

[1] A. Hubert and R. Schäfer, *Magnetic Domains* (Springer, Berlin, 1998).
[2] S. McVitie, G. S. White, J. Scott, P. Warin, and J. N. Chapman, J. Appl. Phys. **90**, 5220 (2001).
[3] C. M. Schneider, R. Frömter, C. Ziethen, G. Schönhense, and J. Kirschner, Synchrotron Radiation News **10**, 22 (1997).
[4] M. Kleiber, M. Bode, R. Ravlic, and R. Wiesendanger, Phys. Rev. Lett. **85**, 4606 (2000).
[5] M. Kleiber, M. Bode, R. Ravlic, N. Tezuka, and R. Wiesendanger, J. Magn. Magn. Mater. **240**, 64 (2002).
[6] S. Anders, H. Padmore, R. Duarte, T. Renner, T. Stammler, A. Scholl, M. Scheinfein, J. Stöhr, L. Séve, and B. Sinkovic, Rev. Sci. Instrum. **70**, 3973 (1999).
[7] G. van der Laan, J. Zaanen, G. Sawatzky, R. Karnatak, and J.-M. Esteva, Phys. Rev. B **33**, 4253 (1986).
[8] D. Alders, J. Vogel, C. Levelut, S. Peacor, T. Hibma, M. Sacchi, L. Tjeng, G. van der Laan, B. Thole, and G. Sawatzky, Europhys. Lett. **32**, 259 (1995); Phys. Rev. B **57**, 11623 (1998).
[9] A. Scholl, J. Stöhr, J. Lüning, J. W. Seo, J. Fompeyrine, H. Siegwart, J. P. Locquet, F. Nolting, S. Anders, E. E. Fullerton, M. R. Scheinfein, and H. A. Padmore, Science **287**, 1014 (2000).
[10] H. Ohldag, N. Weber, C. Bethke, U. Mick, and F. U. Hillebrecht, Synchrotron Radiation News **13**, 25 (2000).
[11] F. U. Hillebrecht, H. Ohldag, N. B. Weber, C. Bethke, U. Mick, M. Weiss, and J. Bahrdt, Phys. Rev. Lett. **86**, 3419 (2001).
[12] For region 2, we obtain the following widths (from left to right): 164 nm, 225 nm (this large width is an artifact resulting from the kink in the wall within the sampled region), 184 nm (profile given in top panel of Fig. 2). Region 3: 140 nm, 159 nm, 179 nm.
[13] L. Bartel and B. Morosin, Phys. Rev. B **3**, 1039 (1971).
[14] K. Nakahigashi, N. Fukuoka, and Y. Shimomura, J. Phys. Soc. Jpn. **38**, 1634 (1975).
[15] M. Kléman, J. Appl. Phys. **45**, 1377 (1974).
[16] M. T. Hutchings and E. J. Samuelsen, Phys. Rev. B **6**, 3447 (1972).
[17] T. Yamada, J. Phys. Soc. Jpn. **21**, 650 (1966).
[18] T. Yamada, J. Phys. Soc. Jpn. **21**, 664 (1966).
[19] P. Plessis, S. J. Tonder, and L. Alberts, Solid State Phys. **4**, 1983 (1971).
[20] The finite temperature does not enter explicitly into our modeling. Close to the Neel temperature where M_0 varies noticeably, the energy of the domain wall will vary as M_0^2.